Clustering and Alignment: Understanding the Training Dynamics in Modular Addition

Tiberiu Musat
ETH Zürich
tmusat@ethz.ch

Abstract

Recent studies have revealed that neural networks learn interpretable algorithms for many simple problems. However, little is known about how these algorithms emerge during training. In this article, I study the training dynamics of a small neural network with 2-dimensional embeddings on the problem of modular addition. I observe that embedding vectors tend to organize into two types of structures: grids and circles. I study these structures and explain their emergence as a result of two simple tendencies exhibited by pairs of embeddings: clustering and alignment. I propose explicit formulae for these tendencies as interaction forces between different pairs of embeddings. To show that my formulae can fully account for the emergence of these structures, I construct an equivalent particle simulation where I show that identical structures emerge. I discuss the role of weight decay in my setup and reveal a new mechanism that links regularization and training dynamics. To support my findings, I also release an interactive demo available at https://modular-addition.vercel.app/.

1 Introduction

Mechanistic interpretability aims at reverse-engineering the inner workings of trained neural networks and explaining their behavior in terms of interpretable algorithms. Recent work in this field was very successful in uncovering the algorithms learned by neural networks on simple problems. Zhong et al. [2023] showed that transformers learn to solve modular addition by forming circular structures in the embedding space and applying one of two simple algorithms: a "Clock" algorithm (resembling the way humans read the clock) and a "Pizza" algorithm (unfamiliar, but interpretable; also encountered in this article). Charton [2024] showed that transformers learn to compute the greatest common divisor by identifying the prime factors of the numeric base from the last digits of each number. Quirke and Barez [2024] uncovered that transformers break down the multi-digit addition task into parallel, digit-specific streams, using different algorithms for various digit positions.

However, it remains an open problem to provide a similarly high degree of interpretability for the training dynamics that lead to the emergence of these algorithms. Currently, the most successful approach to understanding the learning process is by uncovering hidden progress measures that increase abruptly during training [Barak et al., 2022]. For example, by constructing two progress measures for the problem of modular addition, Nanda et al. [2023] find that training of neural networks on modular addition can be split into three phases: memorization, circuit formation, and cleanup. While insightful, such methods provide only a high-level description of the training process, without offering a clear explanation of the underlying optimization dynamics. A better understanding of neural networks could lead to AI systems that are more interpretable, more efficient, and more reliable [Doshi-Velez and Kim, 2017, Olah et al., 2020].

Interpretable AI: Past, Present and Future Workshop at NeurIPS 2024

2 My contribution

In this article, I study the training dynamics of a small neural network on the problem of modular addition. My architecture consists in a simplified single-layer transformer with constant attention and 2-dimensional embeddings. My contributions are the following.

Grids and circles I show that embedding vectors tend to organize themselves into circular and grid-like structures, as depicted in Figure 1. The emergence of circular and grid-like structures is consistent with the findings of Zhong et al. [2023], Gromov [2023] and Liu et al. [2022]. I show that grids and circles play a key role in the generalization performance of the model. I also show that weight decay plays a crucial role in the emergence of circular structures and in reducing grid imperfections.

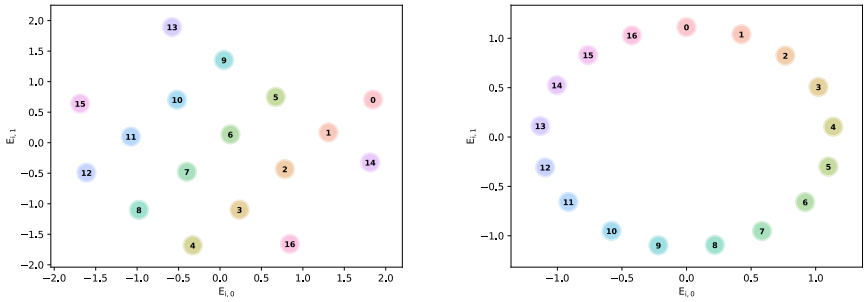

Figure 1: Embedding vectors self-organize into grids (left) and circles (right).

Clustering and alignment I show how grids and circles facilitate accurate classification for the subsequent layers by grouping "pair sums" (outputs of the constant attention). I propose an explanation for the emergence of the grids and circles as a result of two simple phenomena: clustering and alignment. I propose explicit formulae for both phenomena as interaction forces between two different pairs of embeddings.

Particle simulation To prove that my proposed formulae can fully account for the emergence of grids and circles, I construct a particle simulation where particles correspond to embedding vectors and forces correspond to gradients. Forces are computed using only my proposed formulae for clustering and alignment. In this simulation, I show that the particles self-organize into the same structures as the embeddings in the trained transformer: circles, grids, and imperfect grids.

I also contribute to the understanding of weight decay by discussing its role in my particular setup in Appendix C. I also release an interactive demo to allow the readers to explore the training dynamics and particle simulations for themselves: `https://modular-addition.vercel.app/`.

3 Architecture

In this article, I study a simplified single-layer transformer with constant attention. A similar setup has been previously used by Liu et al. [2022], Zhong et al. [2023] and Hassid et al. [2022].

The input to the model consists of two tokens a and b representing the two numbers to be added, where $a, b \in \{0, 1, \ldots, N-1\}$. The tokens are embedded into vectors x_a and x_b using an embedding matrix $E \in \mathbb{R}^{N \times D}$, where D is the embedding dimension. For the scope of this article, I focus on the case when $D = 2$ for simplicity and ease of visualization. Then, a constant attention mechanism is applied to the embeddings. This is equivalent to computing the sum of the embedding vectors.

Then I apply a linear layer of size H with weight matrix $W_h \in \mathbb{R}^{H \times D}$, bias vector $b_h \in \mathbb{R}^H$, and ReLU activation. Finally, I apply a linear layer of size N with a weight matrix $W_o \in \mathbb{R}^{N \times H}$ and bias vector $b_o \in \mathbb{R}^N$. The output of the model is the logits of the predicted sum. I don't use any skip connections or normalization layers.

We can formalize the model as follows:

- Inputs: $a, b \in \{0, 1, \ldots, N-1\}$
- Embeddings: $x_a = E_a$, $x_b = E_b$
- Constant attention: $x = x_a + x_b$
- Linear layer: $h = \mathrm{ReLU}(W_h x + b_h)$
- Output layer: $o = W_o h + b_o$

I train the model in full batch mode using the Adam optimizer with a learning rate of 0.01 and decoupled weight decay [Loshchilov and Hutter, 2019] between 0 and 1. I use the cross-entropy loss. Unless specified, I use $N = 17$ and $H = 32$. The training set consists of 80% of all $N(N+1)/2$ distinct pairs of numbers, chosen randomly. The validation set consists of the remaining 20%.

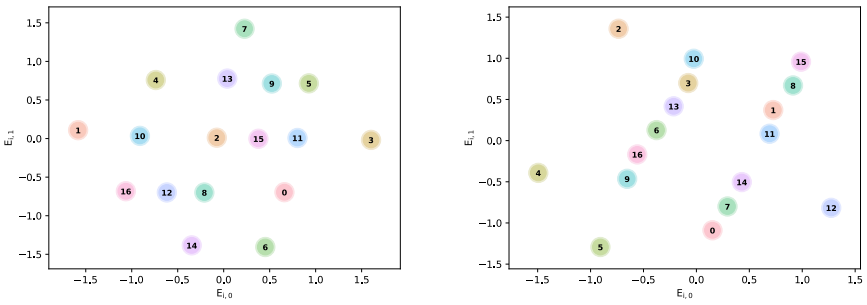

Figure 2: Sometimes embedding vectors self-organize into imperfect grids.

4 Grids and circles: the key to successful generalization

In trained models, the embedding vectors tend to be positioned in arithmetic progressions, forming either grids or circles. I visualize two examples of these structures in Figure 1. The validation accuracy is highest when the embeddings form these structures most clearly. Sometimes, however, the embeddings self-organize into imperfect grids, as shown in Figure 2. In such cases, the validation accuracy is lower, but still higher than when the embeddings are not aligned at all. We present more examples of these structures in Appendix D.

To quantify this effect, I devise two simple algorithms: one to detect circles, and another to quantify the number of grid imperfections in non-circular structures. Both algorithms are explained in detail in the Appendix A.

Table 1: Validation accuracy and structures formed by embedding vectors.

	Circles		Non-Circles			
Weight Decay	Num	Acc	Num	Acc	Grid Imperfections	Correlation
0.0	0	-	100	18.2	102.2 ± 6.1	-0.92 [-0.95, -0.88]
0.3	1	77.4	99	34.8	72.7 ± 6.6	-0.90 [-0.93, -0.85]
0.6	12	65.9	88	51.6	39.6 ± 4.0	-0.84 [-0.89, -0.77]
1.0	18	60.4	82	46.7	31.6 ± 4.0	-0.64 [-0.75, -0.49]

Explanation: I train 100 random initializations for 2000 epochs for various values of weight decay. For each value of weight decay, I report the following: the number of circles and their average validation accuracy, the number of non-circles and their average validation accuracy, the average number of grid imperfections for non-circles, and the correlation between the number of grid imperfections and the validation accuracy of non-circles. For circle detection and grid imperfections, see Appendix A.

I run multiple experiments for various values of weight decay and measure the average validation accuracy of circles and non-circles, as well as the correlation between the validation accuracy and the number of grid imperfections of non-circles. I find that circles consistently have higher validation accuracy than non-circles. For non-circles, I find a strong negative correlation between the number of grid imperfections and the validation accuracy.

5 Co-evolution of embeddings and linear layers

In this section, I will model the training process as the co-evolution of two systems: the embeddings and the subsequent layers. The constant attention mechanism sums the embedding vectors to obtain $x = E_a + E_b$. The subsequent layers then act as a classifier, trying to classify this value as $c = a + b \pmod N$ out of N possible values.

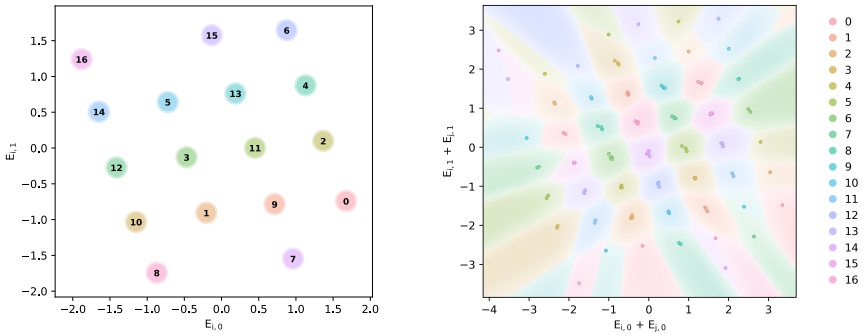

Figure 3: Embedding vectors (left); classifier formed by the combined linear and output layers (background, right) and sums of embedding pairs in the training set (markers, right).

5.1 Clustering

As depicted in Figure 3, the pair sums tend to cluster based on their modular sum. I present more examples in Appendix F. Let's try to understand this phenomenon by considering the interaction between two pair sums $x_{ij} = E_i + E_j$ and $x_{kl} = E_k + E_l$, where $i, j, k, l \in \{0, 1, \ldots, N-1\}$, and (i, j) and (k, l) are two distinct pairs of numbers in the training set.

Let's first consider the case when $i + j \not\equiv k + l \pmod N$. For simplicity, let's assume that there are no other pair sums in between x_{ij} and x_{kl}. In this case, to classify x_{ij} and x_{kl} correctly, the classifier must place a decision boundary between them. This decision boundary will create a gradient that will push x_{ij} and x_{kl} away from each other. Moreover, the closer x_{ij} and x_{kl} are, the narrower the decision boundary will have to be, resulting in a stronger gradient and a stronger push. In other words, the push will be inversely proportional to the distance between the pair sums. I propose the following formula for the gradient at x_{ij} induced by the pair sum x_{kl}:

$$g_{ij \leftarrow kl} = g_r \cdot \frac{x_{ij} - x_{kl}}{\|x_{ij} - x_{kl}\|} \cdot \frac{1}{\|x_{ij} - x_{kl}\|} \tag{1}$$

where g_r is a repulsion constant. The gradient at x_{kl} is defined analogously: $g_{kl \leftarrow ij} = -g_{ij \leftarrow kl}$.

Now, let's consider the case when $i + j \equiv k + l \pmod N$. Again, for simplicity, let's assume that there are no other pair sums in between x_{ij} and x_{kl}. In this case, x_{ij} and x_{kl} are likely to be inside the same classification region. Both pair sums will be attracted towards the point of maximum classification accuracy, which on average will be the center of the classification region. I will model this case with a constant gradient towards the other pair sum:

$$g_{ij \leftarrow kl} = -g_a \cdot \frac{x_{ij} - x_{kl}}{\|x_{ij} - x_{kl}\|} \tag{2}$$

where g_a is an attraction constant. The gradient at x_{kl} is defined analogously: $g_{kl \leftarrow ij} = -g_{ij \leftarrow kl}$. Similar interactions have been previously studied by Baek et al. [2024], Liu et al. [2022], and van Rossem and Saxe [2024].

5.2 Alignment

A different picture emerges when we look at a model where the embeddings form a circle. In Figure 4, I visualize the embedding vectors, pair sums, and the classification function of a model with circular embeddings at the end of training. Pair sums are no longer clustered. Rather, they are aligned along lines that pass through the origin. In this arrangement, the classification regions are skewed and start from the origin, resembling a pizza. This model corresponds exactly to the "pizza" algorithm described by Zhong et al. [2023].

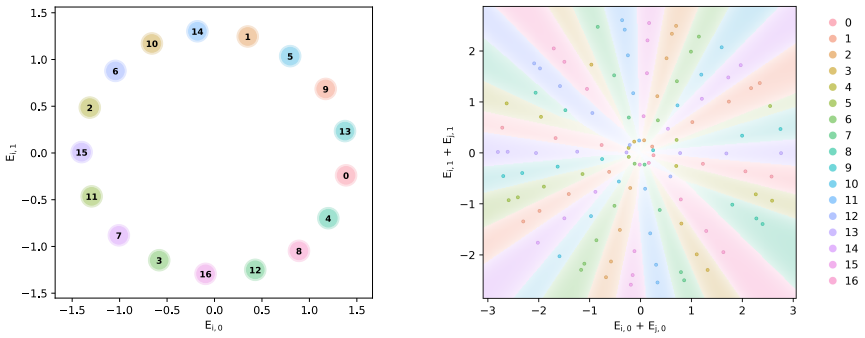

Figure 4: Embedding vectors (left); classifier formed by the combined linear and output layers (background, right) and sums of embedding pairs in the training set (markers, right).

In Table 1, we saw that weight decay plays a crucial role in the emergence of circular structures. To understand the mechanism behind the alignment, we need to consider that the classification function is just a sum of ReLU activations of the linear layer.

Weight decay encourages the linear layer to have small weights and biases, which results in linear functions with small slopes and close to the origin. We explore the precise impact of weight decay on the magnitude of the weights and biases in Appendix B. The only aspect that remains completely unconstrained in the direction of the weight vectors. A weight vector aligned with a specific pair sum is maximally useful for the classification layer because it outputs the maximum possible value for that pair sum and the minimum possible value for the other pair sums. Thus, under these conditions, in order to minimize the training loss, the weight vectors of the linear layer will tend to align with the pair sums.

We can model this behavior as follows. For a single pair sum $x_{kl} = E_k + E_l$, let's consider a linear function with zero bias ($b = 0$) and a weight vector of constant norm that is perfectly aligned with the pair sum ($w = f_a \cdot \frac{x_{kl}}{\|x_{kl}\|}$, where f_a is a constant). After applying the ReLU activation, the output becomes zero for all points x that oppose the direction of x_{kl} (i.e., $x \cdot x_{kl} < 0$). For the other points, the function will have a constant slope of f_a in the direction of x_{kl}.

Inspired by this simplified model, I propose the following formula for the gradient at x_{ij} produced by the pair sum x_{kl}:

$$g_{ij \leftarrow kl} = \begin{cases} 0, & \text{if } x_{ij} \cdot x_{kl} \leq 0 \\ f_a \cdot \frac{x_{kl}}{\|x_{kl}\|}, & \text{if } x_{ij} \cdot x_{kl} > 0 \text{ and } i + j \equiv k + l \pmod{N} \\ -f_a \cdot \frac{x_{kl}}{\|x_{kl}\|}, & \text{if } x_{ij} \cdot x_{kl} > 0 \text{ and } i + j \not\equiv k + l \pmod{N} \end{cases} \tag{3}$$

6 Particle simulation

In this section, I show that my proposed model can fully account for the emergence of the grids and circles by constructing a particle simulation and showing that particles converge to the same structures as the embedding vectors in the trained transformer.

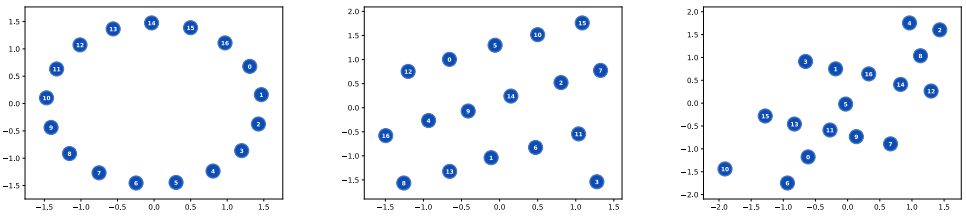

Figure 5: Particles form circles (left), grids (center), and imperfect grids (right).

I model the training dynamics of the embedding vectors using N particles in a D-dimensinal space ($N = 17, D = 2$). I denote the position of particle i by $x_i \in \mathbb{R}^D$, $i = 1, \ldots, N$. The position x_i of particle i corresponds to the embedding vector E_i of the number i during training.

The gradient equations from the previous section become "forces" acting on the N particles. Let (i, j) and (k, l) be two distinct pairs of numbers. I denote the sums of their particle positions as $x_{ij} = x_i + x_j$ and $x_{kl} = x_k + x_l$, respectively. The pair (k, l) will induce an equal force on particles i and j (obtained by combining equations 1, 2, and 3):

$$F_i = F_j = \begin{cases} g_a \cdot \frac{x_{kl} - x_{ij}}{\|x_{kl} - x_{ij}\|} & \text{if } x_{ij} \cdot x_{kl} \leq 0 \text{ and } i + j \equiv k + l \pmod{N} \\ g_r \cdot \frac{x_{ij} - x_{kl}}{\|x_{ij} - x_{kl}\|^2} & \text{if } x_{ij} \cdot x_{kl} \leq 0 \text{ and } i + j \not\equiv k + l \pmod{N} \\ g_a \cdot \frac{x_{kl} - x_{ij}}{\|x_{kl} - x_{ij}\|} + f_a \cdot \frac{x_{kl}}{\|x_{kl}\|} & \text{if } x_{ij} \cdot x_{kl} > 0 \text{ and } i + j \equiv k + l \pmod{N} \\ g_r \cdot \frac{x_{ij} - x_{kl}}{\|x_{ij} - x_{kl}\|^2} - f_a \cdot \frac{x_{kl}}{\|x_{kl}\|} & \text{if } x_{ij} \cdot x_{kl} > 0 \text{ and } i + j \not\equiv k + l \pmod{N} \end{cases}$$

The force acting on particles k and l is defined analogously. I use $g_r = g_a = f_a = 1$. Forces are weighted so that interactions between pair sums of different modular sum have the same total contribution as those between pair sums of the same modular sum. Particles are initialized randomly according to a normal distribution. At every step of the simulation, the total force acting on each particle is calculated. The, each particle is moved with a small step in the direction of the total force. I also scale the particle positions to maintain a constant variance and zero mean. I repeat this process for 100 steps. No momentum is used.

I observe that the particles self-organize into the same structures as the embeddings in the trained transformer: circles, grids, and imperfect grids. We visualize a few examples in Figure 5. For more examples, see Appendix E. In Table 2, we present the results of running 100 simulations for various values of f_a. We find that the relative frequency of circles and the average number of grid imperfections are very similar to the results obtained from the transformer experiments. I also find that increasing f_a leads to more circles, which is consistent with my hypothesis that circles emerge as a result of the alignment force.

Table 2: Results of particle simulations for various values of f_a

f_a	Number of Circles	Number of Grids	Average Grid Imperfections
0.5	0	100	35.5 ± 3.7
1.0	17	83	36.3 ± 4.8
2.0	56	44	42.9 ± 10.1

7 Conclusion

I have explained the training dynamics of a simplified transformer on the problem of modular addition in terms of two simple phenomena: clustering and alignment. I have provided strong empirical evidence for my model using a particle simulation. I have also provided a qualitative argument for the two phenomena, but further work is needed to fully understand their origin.

References

M. Andriushchenko, F. D'Angelo, A. Varre, and N. Flammarion. Why do we need weight decay in modern deep learning? *arXiv preprint arXiv:2310.04415*, 2023.

D. D. Baek, Z. Liu, and M. Tegmark. Geneft: Understanding statics and dynamics of model generalization via effective theory. *arXiv preprint arXiv:2402.05916*, 2024.

B. Barak, B. Edelman, S. Goel, S. Kakade, E. Malach, and C. Zhang. Hidden progress in deep learning: Sgd learns parities near the computational limit. In S. Koyejo, S. Mohamed, A. Agarwal, D. Belgrave, K. Cho, and A. Oh, editors, *Advances in Neural Information Processing Systems*, volume 35, pages 21750–21764. Curran Associates, Inc., 2022. URL https://proceedings.neurips.cc/paper_files/paper/2022/file/884baf65392170763b27c914087bde01-Paper-Conference.pdf.

F. Charton. Learning the greatest common divisor: explaining transformer predictions. 2024.

F. Doshi-Velez and B. Kim. Towards a rigorous science of interpretable machine learning. 2017.

I. Goodfellow, Y. Bengio, and A. Courville. *Deep Learning*. MIT Press, 2016. http://www.deeplearningbook.org.

A. Gromov. Grokking modular arithmetic. 2023.

M. Hassid, H. Peng, D. Rotem, J. Kasai, I. Montero, N. A. Smith, and R. Schwartz. How much does attention actually attend? questioning the importance of attention in pretrained transformers. In Y. Goldberg, Z. Kozareva, and Y. Zhang, editors, *Findings of the Association for Computational Linguistics: EMNLP 2022*, pages 1403–1416, Abu Dhabi, United Arab Emirates, Dec. 2022. Association for Computational Linguistics. doi: 10.18653/v1/2022.findings-emnlp.101. URL https://aclanthology.org/2022.findings-emnlp.101.

A. Krogh and J. Hertz. A simple weight decay can improve generalization. *Advances in neural information processing systems*, 4, 1991.

Z. Liu, O. Kitouni, N. S. Nolte, E. Michaud, M. Tegmark, and M. Williams. Towards understanding grokking: An effective theory of representation learning. *Advances in Neural Information Processing Systems*, 35:34651–34663, 2022.

I. Loshchilov and F. Hutter. Decoupled weight decay regularization. In *International Conference on Learning Representations*, 2019. URL https://openreview.net/forum?id=Bkg6RiCqY7.

N. Nanda, L. Chan, T. Lieberum, J. Smith, and J. Steinhardt. Progress measures for grokking via mechanistic interpretability. In *The Eleventh International Conference on Learning Representations*, 2023. URL https://openreview.net/forum?id=9XFSbDPmdW.

C. Olah, N. Cammarata, L. Schubert, G. Goh, M. Petrov, and S. Carter. Zoom in: An introduction to circuits. *Distill*, 2020. doi: 10.23915/distill.00024.001. https://distill.pub/2020/circuits/zoom-in.

P. Quirke and F. Barez. Understanding addition in transformers. In *The Twelfth International Conference on Learning Representations*, 2024. URL https://openreview.net/forum?id=rIx1YXVWZb.

L. van Rossem and A. M. Saxe. When representations align: Universality in representation learning dynamics. *arXiv preprint arXiv:2402.09142*, 2024.

G. Zhang, C. Wang, B. Xu, and R. Grosse. Three mechanisms of weight decay regularization. *arXiv preprint arXiv:1810.12281*, 2018.

Z. Zhong, Z. Liu, M. Tegmark, and J. Andreas. The clock and the pizza: Two stories in mechanistic explanation of neural networks. In A. Oh, T. Neumann, A. Globerson, K. Saenko, M. Hardt, and S. Levine, editors, *Advances in Neural Information Processing Systems*, volume 36, pages 27223–27250. Curran Associates, Inc., 2023. URL https://proceedings.neurips.cc/paper_files/paper/2023/file/56cbfbf49937a0873d451343ddc8c57d-Paper-Conference.pdf.

A Algorithms

A.1 Circle detection

To determine whether the embedding vectors form a circle, I simply consider the ratio of the maximum and minimum distances of the embeddings to the origin. If the ratio is below a certain threshold, I consider the embeddings to form a circle. I use a threshold value of 1.2. For my setup, I observe that this simple algorithm is sufficient to detect circles with great accuracy.

Algorithm 1 Check if Embeddings Form a Circle

function IS_CIRCLE(E: embedding matrix)
    $min\_norm \leftarrow \min(\sqrt{x^2+y^2} \mid (x,y) = E_i, i \in \{0,\ldots,N-1\})$
    $max\_norm \leftarrow \max(\sqrt{x^2+y^2} \mid (x,y) = E_i, i \in \{0,\ldots,N-1\})$
    return $max\_norm/min\_norm < 1.2$
end function

A.2 Grid imperfections

I propose a simple measure to quantify the number of grid imperfections inspired by the following fact: in a perfect grid, the vector sums of all pairs of embeddings also form a perfect grid where pair sums are grouped together based on their modular sum.

My measure works as follows. For each pair of embeddings (E_i, E_j), I find the pair of embeddings (E_k, E_l) with the closest vector sum. If the modular sum $(i+j) \bmod N$ is different from the modular sum $(k+l) \bmod N$, I consider this pair to be an "imperfection".

Algorithm 2 Count Grid Imperfections in Embedding

function IMPERFECTIONS(E: embedding matrix)
    $N \leftarrow \text{len}(embed)$
    $pairs \leftarrow \{(i,j) \mid i \in \{0,\ldots,N-1\}, j \in \{i,\ldots,N-1\}\}$
    $imperfections \leftarrow 0$
    for all $(i,j) \in pairs$ **do**
        $min\_dist \leftarrow \infty$
        $match \leftarrow$ False
        for all $(k,l) \in pairs$ **do**
            if $(i,j) = (k,l)$ **then**
                continue
            end if
            $dist \leftarrow \|E_i + E_j - E_k - E_l\|$
            if $dist < min\_dist$ **then**
                $min\_dist \leftarrow dist$
                $match \leftarrow i + j \equiv k + l \mod N$
            end if
        end for
        if not $match$ **then**
            $imperfections \leftarrow imperfections + 1$
        end if
    end for
    return $imperfections$
end function

B Weight decay and the magnitude of weights and biases

Below I visualize the magnitude of the weights and biases of the linear layer at the end of training for various values of weight decay. I run 10 random initializations for 2000 epochs with a learning rate of 0.01. I plot the average absolute value of the weights and biases of the linear layers among the 10 runs in Figure 6. We can observe that weight decay strongly limits the magnitude of the weights and biases, with biases being limited more than weights.

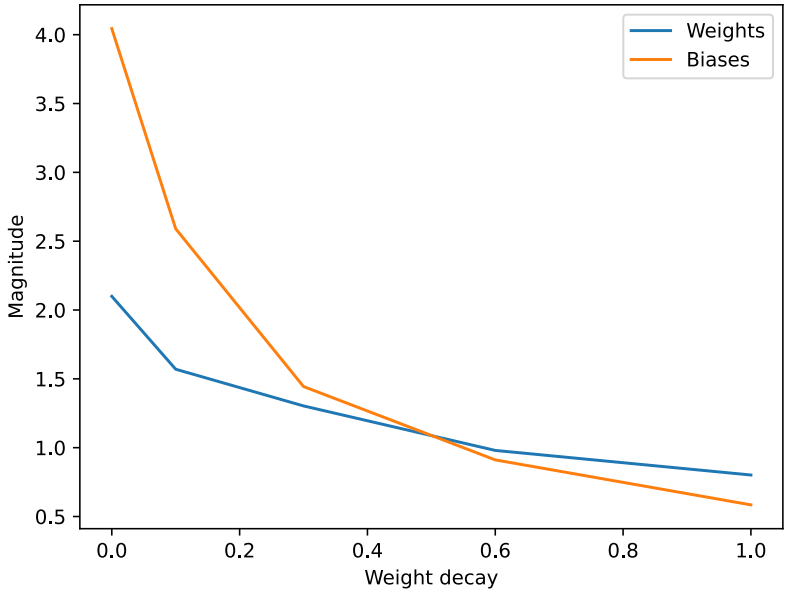

Figure 6: Average magnitude of the weights and biases of the linear layer at the end of training for various values of weight decay.

C The role of weight decay

Weight decay is a broadly used regularization technique for training state-of-the-art deep networks [Loshchilov and Hutter, 2019, Krogh and Hertz, 1991, Andriushchenko et al., 2023]. Weight decay penalizes large weights and biases by applying an exponential decay to each parameter (θ) at every step of the optimization. The decay rate is proportional to the learning rate (λ) and the weight decay coefficient (γ), as shown in the following formula:

$$\theta_{t+1} \leftarrow \theta_t - \lambda\gamma\theta_t \tag{4}$$

Traditionally, weight decay was understood as a form of L_2 regularization, improving generalization by constraining the network capacity [Goodfellow et al., 2016]. More recently, a new perspective on weight decay has emerged, suggesting that it plays a much more important role during training by changing the training dynamics in a desirable way [Zhang et al., 2018]. In this section, I combine the two perspectives by discussing the impact of weight decay on the training dynamics in my setup.

In Section 4, we observed that weight decay plays an important role in the successful generalization of the trained model. I propose the following explanation: weight decay changes the training dynamics by strengthening the clustering force and by introducing the alignment force. In turn, these forces facilitate the emergence of grids and circles, which are crucial for the generalization performance of the model. Below I discuss exactly how weight decay impacts clustering and alignment.

In the case of clustering, my proposed clustering force (Equations 1 and 2) is highly dependent on a simplified model of the classification function where the decision boundaries are very wide. Weight decay enables this by limiting the magnitude of the weights of the linear layer and output layer, as I show in Appendix B. Without weight decay, classification boundaries could get arbitrarily narrow, leading to a clustering force that is very strong in a narrow region, but practically non-existent elsewhere. In other words, without weight decay, the classifier would overfit to the pair sums and the embeddings would become stuck in a local minimum.

In the case of alignment, weight decay makes the alignment force (Equation 3) possible by limiting the magnitude of the biases of the linear layer, as I show in Appendix B. This forces the ReLU activations of the linear layer to remain very close to the origin, creating the sort of alignment we have seen. Without weight decay, biases could get arbitrarily large and there would not be any specific point around which the alignment could take place.

This represents a very interesting link between regularization and training dynamics. By regularizing one part of the model, we enable the emergence of desirable training dynamics in another part of the model. Without weight decay, a layer could overfit to the current state of the other layers, limiting them from making further progress. This could explain why weight decay is so effective in training deep learning models [Andriushchenko et al., 2023], which consist of many different layers that need to co-evolve harmoniously during training.

To the best of my knowledge, this link between regularization and training dynamics has not been previously reported. This opens up interesting new questions for future research, such as providing theoretical proof for this phenomenon or showing how it takes place in other problems and architectures.

D Embedding vectors

Below I visualize the embedding vectors that emerge from several random initializations in the trained transformer for various values of weight decay, after training for 2000 epochs with a learning rate of 0.01.

D.1 Weight decay $= 1.0$

D.2 Weight decay = 0.6

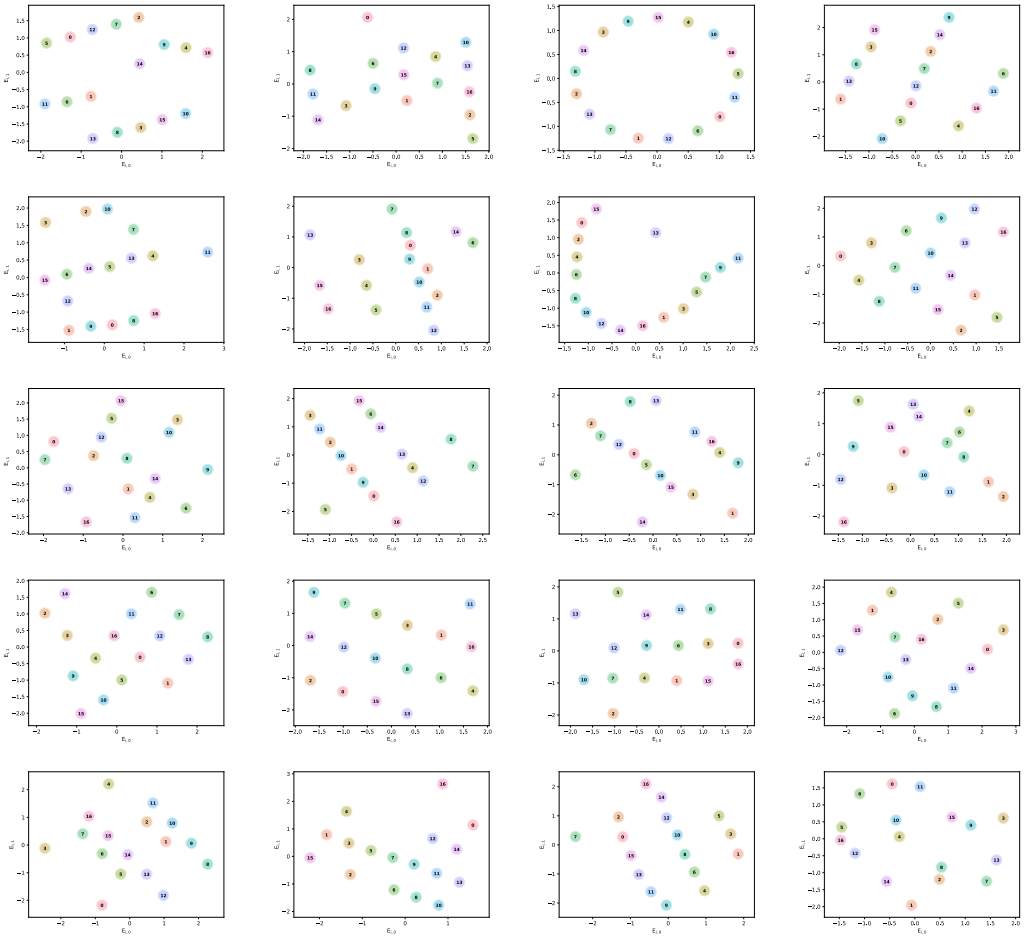

D.3 Weight decay = 0.3

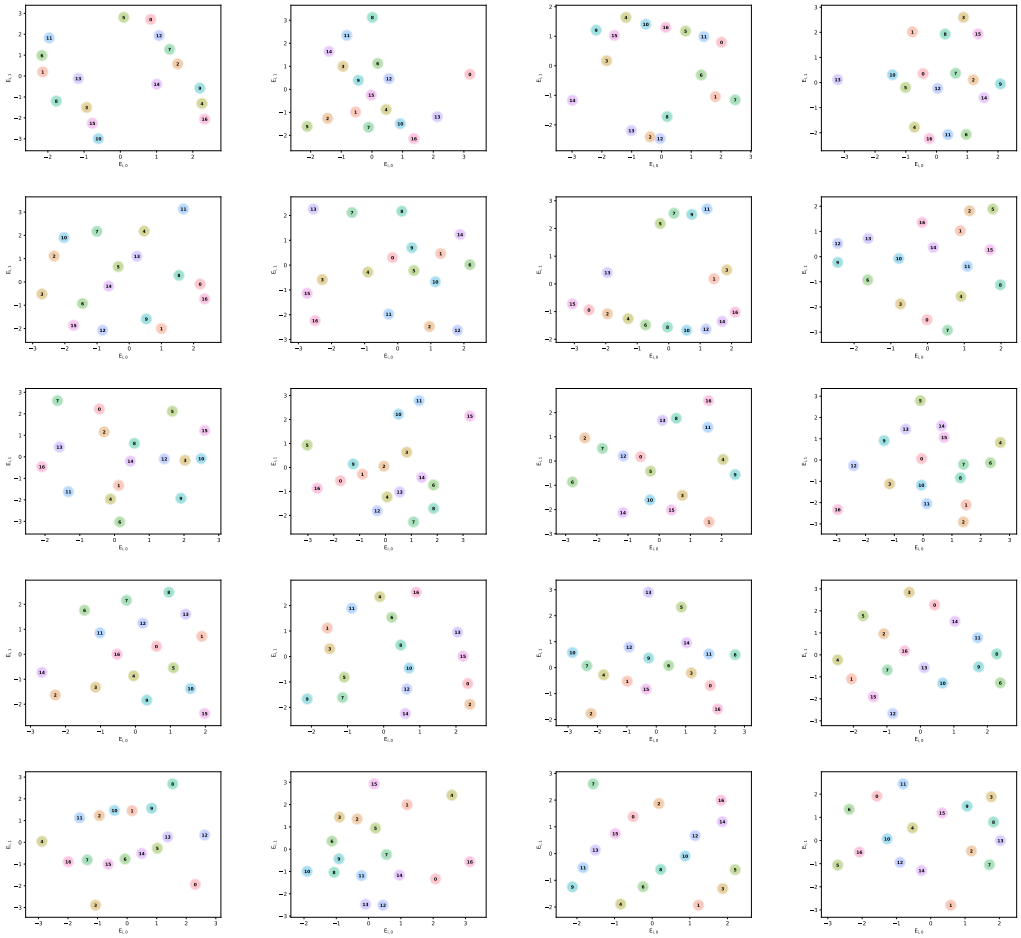

D.4 Weight decay = 0.0

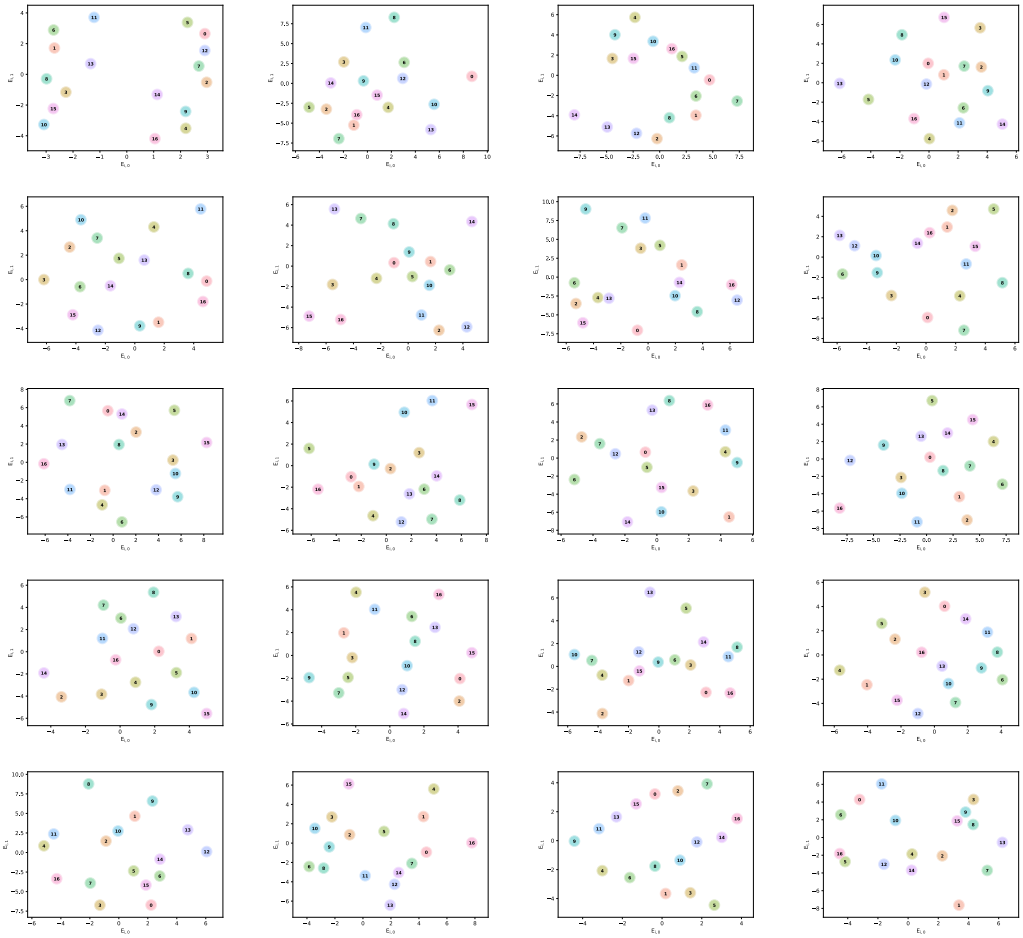

E Particle simulation

Below I visualize several particle arrangements that emerge from different random initializations in the particle simulation for various values of f_a, after running the simulation for 100 steps. I maintain $N = 17, D = 2, g_r = g_a = 1$.

E.1 $f_a = 1.0$

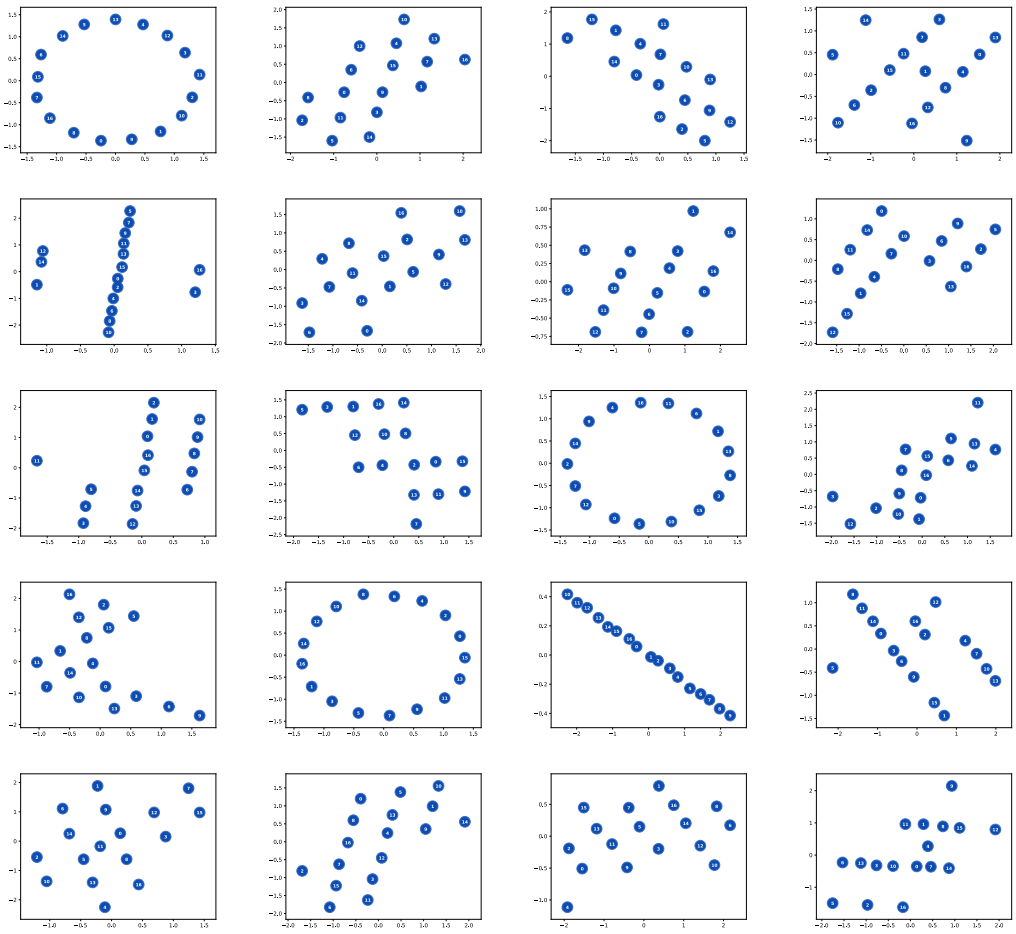

E.2 $f_a = 2.0$

E.3 $f_a = 0.5$

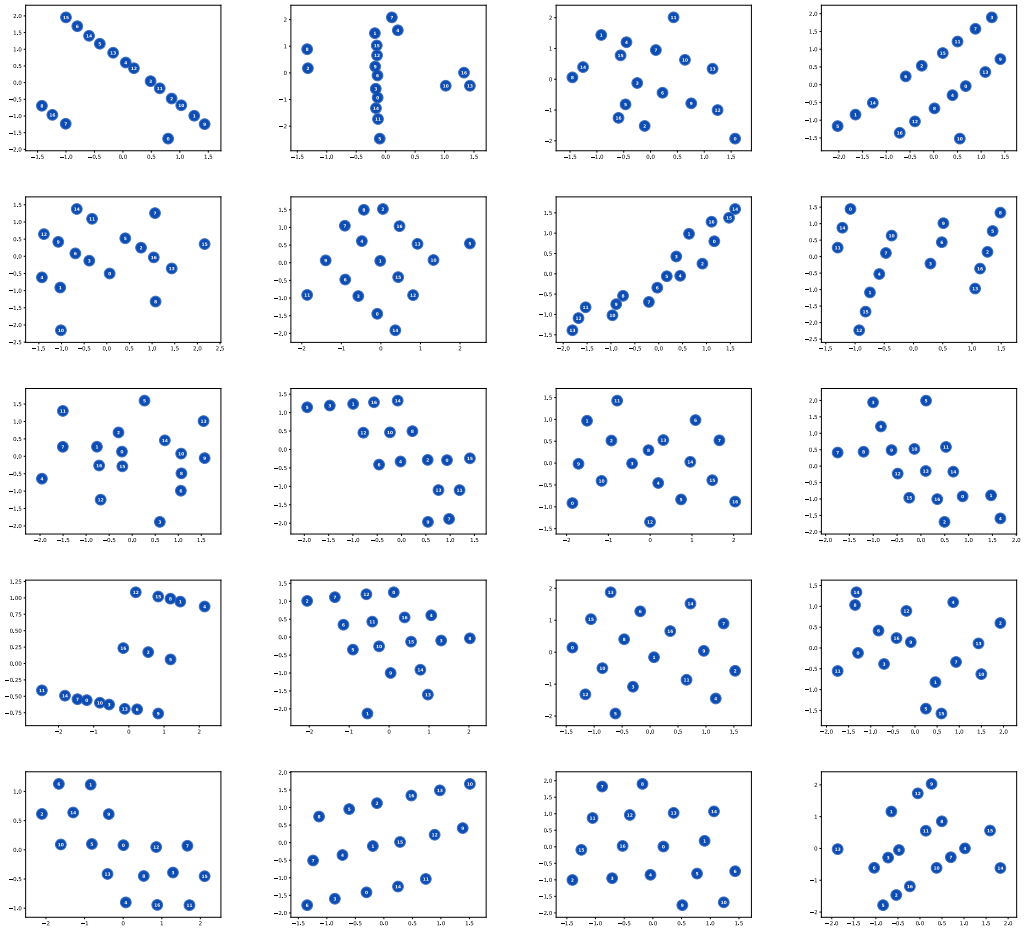

F Classifier visualization

Below I visualize the embedding vectors (left) and the classification function formed by the subsequent layers (right) of several models at the end of training. In the right plot, I also plot the sums of the embedding vectors of all pairs in the training set ("pair sums"). Models were trained for 2000 epochs with a learning rate of 0.01 and a weight decay of 0.6.

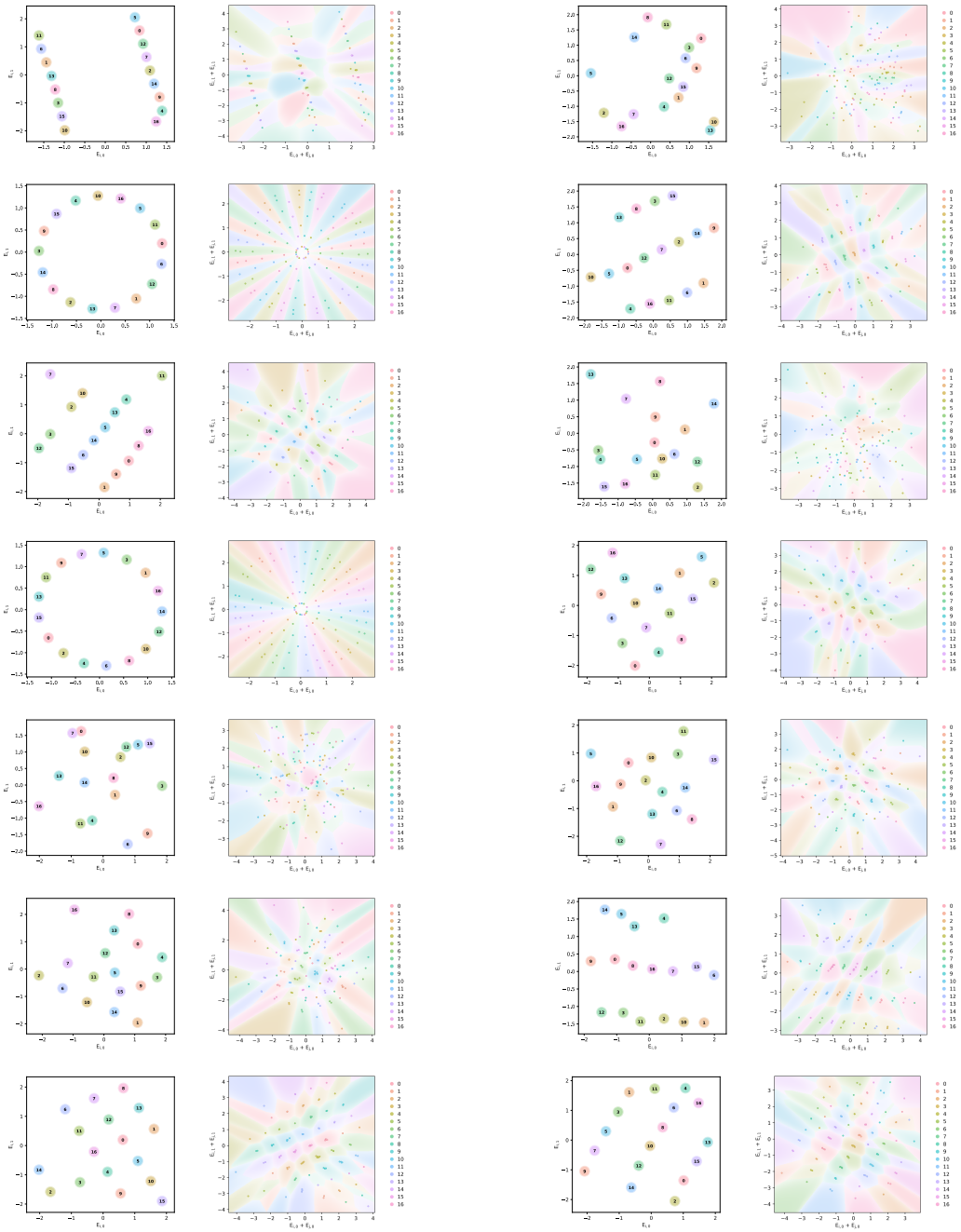

G Embedding vectors in 3D and 4D

Below I visualize the embedding vectors that emerge from several random initializations in the trained transformer with 3-dimensional and 4-dimensional embeddings. I train for 2000 epochs with a weight decay of 1 and a learning rate of 0.01.

I use three 2D plots to visualize each configuration of embeddings. I project the embeddings onto pairs of dimensions and plot the resulting 2D projections. It is not possible to visualize 3D and 4D embeddings directly, but we can still get a sense of their grid-like or circular structure by examining the 2D projections.

G.1 3-dimensional embeddings

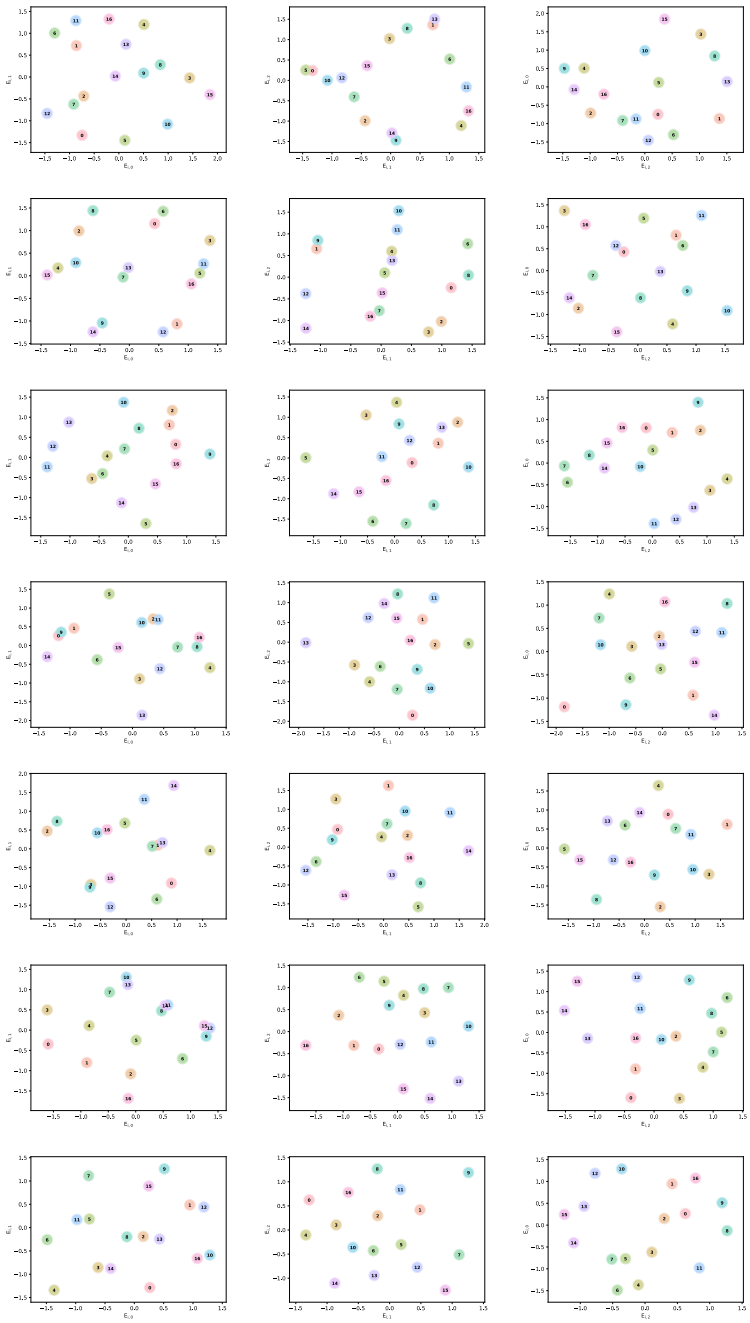

G.2 4-dimensional embeddings